

Variability in the massive black hole binary candidate SDSS J2320+0024: no evidence for periodic modulation

Fabio Rigamonti^{1,2,4,*}, Lorenzo Bertassi³, Riccardo Buscicchio^{3,2}, Fabiola Cocchiararo^{3,2}, Stefano Covino^{1,4},
Massimo Dotti^{3,1,2}, Alberto Sesana^{3,1,2}, and Paola Severgnini¹

¹ INAF - Osservatorio Astronomico di Brera, via Brera 20, I-20121 Milano, Italy

² INFN, Sezione di Milano-Bicocca, Piazza della Scienza 3, I-20126 Milano, Italy

³ Università degli Studi di Milano-Bicocca, Piazza della Scienza 3, 20126 Milano, Italy

⁴ Como Lake centre for AstroPhysics (CLAP), DiSAT, Università dell'Insubria, via Valleggio 11, 22100 Como, Italy

Received XXX; accepted YYY

ABSTRACT

Massive black hole binaries (MBHBs) are a natural outcome of galaxy mergers, and they are expected to be among the loudest gravitational wave sources at low frequencies. SDSS J2320+0024 has been recently proposed as a promising MBHB candidate due to a possible periodicity in its light-curve and variability in the MgII emission line. In this work, we re-analyse the optical (g and r bands) light-curves of J2320+0024 within the framework of Bayesian model selection. When a periodicity is searched for together with red noise, the analysis of the g-band light-curve finds a peak in the posterior of the period at ~ 290 days. The posterior profile is too broad to result in a preference for the periodic models with respect to models including only red-noise. Furthermore, the same peak is not present in the analysis of the r-band light-curve. A periodic model without red-noise identifies a different (~ 1100 days) periodicity, and it is significantly statistically disfavoured with respect to the other tested models. In summary, no significant evidence in favour of a true periodic signal over red noise variability is found. Our analysis questions the robustness of the previously claimed periodicity and emphasizes the importance of rigorous statistical treatment. While our findings challenge the binary interpretation for J2320+0024, they do not rule it out. A statistically robust joint analysis of the photometric light-curves and of the evolving broad line profiles can shed further light on the real nature of this object.

Key words. galaxies: active - galaxies: interactions - quasars: individual: SDSS J2320+0024 - methods: statistical - methods: data analysis - Techniques: photometric

1. Introduction

In the current picture of hierarchical growth of galaxies, massive black hole (MBH) binaries (MBHBs) are expected to form and be fairly common in our Universe as a consequence of galaxy mergers (Begelman et al. 1980; Volonteri et al. 2016; Rosas-Guevara et al. 2019; De Rosa et al. 2019). The study, characterisation, and identification of these systems from an electromagnetic perspective are of paramount importance in light of current (e.g., pulsar timing array, PTA, Verbiest et al. 2016) and future (e.g., LISA Amaro-Seoane et al. 2017, 2022) gravitational waves (GWs) missions, as these systems are expected to be among the loudest sources of GWs. Still, MBHBs remain observationally elusive as several challenges complicate their unambiguous identification through electromagnetic signatures. In fact, to date, despite the large number of MBHB candidates being put forward, no definite observational confirmation of any of them has been provided, yet. The identification of MBHBs relies on indirect signatures either by searching for peculiar spectral features (Tsalmantza et al. 2011; Eracleous et al. 2012; Ju et al. 2013; Shen et al. 2013; Wang et al. 2017) or through photometric variability in their light-curve (Valtonen et al. 2008; Ackermann et al. 2015; Graham et al. 2015; Li et al. 2016; Charisi et al. 2016; Sandrinelli et al. 2016, 2018; Severgnini et al. 2018; Li et al. 2019; Liu et al. 2019; Chen et al. 2020; Serafinelli et al. 2020; Covino et al. 2019).

The first approach is associated with MBHBs with separations larger than 0.01 pc. At such distances, typically larger than the Roche lobe of the system, the individual MBHBs still retain their own broad line region (BLR) (Montuori et al. 2011, 2012). In these cases, we expect broad emission lines (BELs) to be shifted in frequency with respect to their respective narrow emission lines (NELs) and to evolve in time over a binary orbital period. However, asymmetric emission line profiles can also be explained by complex dynamics and morphology of the BLR (Eracleous et al. 1997; Jovanović et al. 2010; Storch-Bergmann et al. 2003; Rigamonti et al. 2025; Sottocorno et al. 2025). The presence of a SMBHB would be checked by measuring the expected drift in wavelengths over a binary orbital period, i.e. observing the candidate for ≈ 10 yr or longer¹.

The second approach is more suitable for binaries at closer separations, where the individual BLRs are either truncated or shared by both MBHBs. In such configurations, periodic variability over the orbital timescales is expected potentially due to periodic feeding from the circumbinary disc (Hayasaki et al. 2008; Tiede et al. 2024), Doppler boosted emission (D'Orazio et al. 2015), or periodic gravitational lensing (D'Orazio & Di Stefano 2018; Davelaar & Haiman 2022). However, even in that

¹ Notably, a faster test, requiring an observational campaign on timescales comparable to typical reverberation mapping observation, has been proposed by Gaskell (1988) and recently quantitatively detailed by Dotti et al. (2023).

* fabio.rigamonti@inaf.it

situations, convincing evidence that these sources are indeed MBHBs is still missing, both due the theoretical predictions for their emission and the plausibility of alternative interpretations such as the assumption of precession in jets and in the inner part of the accretion discs (Sandrinelli et al. 2016; Britzen et al. 2018). Solving this ambiguity requires alternative approaches, encompassing time domain and spectral analysis, (e.g., Bertassi et al. 2025) to robustly test the binary hypothesis. Finally, the most challenging complication in the identification of genuine MBHBs from light-curve analysis is given by the intrinsic quasar variability. Indeed the light-curves of accreting AGNs generally show correlated red-noise variability with power spectrum well described by a ν^{-2} power-law with a flattening at low frequency, i.e. a damped random walk (DRW, Kelly et al. 2009). Such variability can mimic quasi-periodicities, making actual periodicities difficult to unambiguously identify (Vaughan et al. 2016; Liu et al. 2018; Covino et al. 2019). Multiple objects initially showing an apparent periodicity were later revealed to be non-periodic (Graham et al. 2015; Liu et al. 2018; Jiang et al. 2022; Dotti et al. 2023). Established approaches to assess a source periodicity rely nowadays on Bayesian inference (Covino et al. 2020; Zhu & Thrane 2020).

SDSS J2320+0024 (J2320+0024 hereinafter) has been proposed as a MBHB candidate due to a detected peak ($T \approx 260$ days) in its Lomb-Scargle periodogram (Fatović et al. 2023), possibly coupled with a variability in its Mg II broad emission line (Fatović et al. 2025). However, to date, no rigorous assessment of the significance of the observed periodicity has been provided. In particular, a comparison with quasar red noise and an evaluation within a robust Bayesian framework are still missing. In this study, we aim to test the binary nature of J2320+0024, focusing on the periodicity detected in its light-curve.

In Sec. 2, we briefly present the archival datasets of the MBHB candidate analysed in this paper. We then describe our approach to the analysis of the light-curve of J2320+0024 in Sec. 3, ranking different noise and periodic models with each other. Finally, in Sec. 4 we discuss our results and present our conclusions.

2. Data

J2320+0024 is a system at redshift $z = 1.05$, identified from a long-period variability search in the Sloan Digital Sky Survey Stripe 82 Standards Catalog (SDSS S82, York et al. 2000; Jiang et al. 2014; Ivezić et al. 2007). It was proposed as a MBHB candidate (Fatović et al. 2023) by Fatović et al. (2023), based on time-resolved analysis of its light-curve and, and was later followed up with spectral observation (Fatović et al. 2025). To assess the robustness of the periodicity detection in the light-curve of J2320+0024 we collected g- and r-band magnitudes from the SDSS, Pan-STARRS1 (PS1, Chambers et al. 2016), and Zwicky Transient Facility (ZTF, Graham et al. 2019; Bellm et al. 2019) surveys. Following Fatović et al. (2023), we calibrated the data from the different surveys to the median SDSS flux to empirically account for the instrumental offsets. In the following, we present the analysis on the g-band, while the corresponding results for the r-band are reported in Appendix A.

3. Modelling of the light-curve

As discussed in Sec. 1, Quasi-Stellar Objects (QSOs) are variable sources whose intrinsic variability is typically well described by a DRW (Kelly et al. 2009) model. This model could

mimic a spurious periodic signal (Vaughan et al. 2016), as a random realization of a DRW with a correlation timescale τ can produce few periodic cycles spanning a timescale $\gtrsim \tau$. Therefore, it is extremely challenging to confirm periodicities which are not much shorter than the dataspan (usually one needs several ($O(10)$) periods for a robust claim. This is why robust detection of periodic variability, either associated with the presence of a MBHB (Liu et al. 2018) or with other repeating processes (Covino et al. 2019), is difficult, thus requiring a cautious approach. In what follows, we analyse the light-curves of J2320+0024 within a fully Bayesian framework, modelling the data as realisations from a Gaussian process (GP) and performing model selection over multiple ones.

The same approach has already been proposed in the literature (Covino et al. 2020; Zhu & Thrane 2020; Covino et al. 2022) and constitutes the most reliable solution to quasar light-curve characterization.

3.1. Gaussian Processes and Bayesian Inference

Bayesian analysis of light-curves typically makes use of the GP formalism (Rasmussen & Williams 2006; Roberts et al. 2012; Angus et al. 2018). GPs describe distributions over functions and, in their discretized version, correspond to multivariate Gaussian distributions. GPs offer a flexible framework for modelling unknown time series by non-parametric models capable of capturing a large family of functions with two parameters: a kernel and a mean function. The kernel choice, which defines the GP covariance matrix, regulates the overall shapes and smoothness of samples, i.e. functions. Kernels can be of different functional form, usually depending on a few free (hyper)-parameters, and allowing for the modelling of either periodic or non-periodic light-curves. In the context of Bayesian inference, the identification of the kernel parameters that best describe the observed data passes through the evaluation of the GP log marginal-likelihood, which reads as follows Rasmussen & Williams (2006)

$$\log \mathcal{L}(\mathbf{D}|\mathbf{\Omega}) = -\frac{1}{2}(\mathbf{D}-\boldsymbol{\mu})^T \widetilde{\boldsymbol{\Sigma}}^{-1}(\mathbf{D}-\boldsymbol{\mu}) - \frac{1}{2} \log |\widetilde{\boldsymbol{\Sigma}}| - \frac{N}{2} \log 2\pi, \quad (1)$$

where, in our case, \mathbf{D} is the observed magnitude, $\boldsymbol{\mu}$ is the mean function of the GP, N is the number of observations, $\widetilde{\boldsymbol{\Sigma}}$ is the covariance matrix computed as the squared sum of the GP kernel $\boldsymbol{\Sigma}$ and the diagonal term given by the error measurements, while $|\widetilde{\boldsymbol{\Sigma}}|$ is the covariance matrix determinant. To reduce at minimum the number of free parameters in the model, we standardised (i.e., removed the mean and divided by the standard deviation²) the \mathbf{D} so that we could always assume $\boldsymbol{\mu} = 0$.

In this work, we compared four different kernels typically used to describe periodic and non-periodic light-curves: the exponential kernel DRW, the "Modified DRW" kernel, the "Quasi-periodic oscillation" (QPO) kernel, and the "Periodic" kernel. We refer to Zhu & Thrane (2020) for a detailed discussion.

The DRW model assumes an exponential kernel described by

$$\Sigma_{ij} = \frac{1}{2} \sigma^2 \tau \exp\left(-\frac{|t_i - t_j|}{\tau}\right), \quad (2)$$

where σ is the intrinsic variance, τ is the damping timescale, and t_i is the time at which the i -th observation has been taken.

² The mean g-band magnitude is 21.616 while the standard deviation is 0.319.

Table 1. Summary of the different model parameters for the fit to the g-band light-curve of SDSS J2320+0024.

Description	Name	Prior range	DRW	Modified DRW	QPO	Periodic
50th, 16th, 84th Percentiles						
Scale length	$\log_{10} \tau$	$[-3, 1.7]$	$-1.3^{+0.3}_{-0.2}$	$-1.6^{+0.3}_{-0.2}$	$-1.3^{+0.4}_{-0.3}$	-
Dispersion	$\log_{10} \sigma$	$[-3, 1.7]$	$0.8^{+0.1}_{-0.1}$	$0.9^{+0.1}_{-0.1}$	$0.8^{+0.1}_{-0.1}$	$0.1^{+0.3}_{-0.2}$
Slope	γ	$[0.5, 5]$	-	$1.4^{+0.4}_{-0.4}$	-	-
Period	$\log_{10} T$	$[-2, 2]$	-	-	$0.2^{+1.3}_{-1.3}$	$-0.406^{+0.002}_{-0.002}$
Maximum Likelihood						
Scale length	$\log_{10} \tau$	$[-3, 1.7]$	-1.35	-1.65	-0.74	
Dispersion	$\log_{10} \sigma$	$[-3, 1.7]$	0.79	0.94	0.51	0.02
Slope	γ	$[0.5, 5]$	-	1.51	-	-
Period	$\log_{10} T$	$[-2, 2]$	-	-	-0.99	-0.41
log evidence	$\log Z$	-	-139.15	-139.0	-138.90	-238.60

Notes. From left to right, the columns provide a brief description of each parameter, its reference name as used in this work, the assumed prior range, and the best-fit values with their credibility intervals for all the different models. The first table block reports the parameters estimated as the median, 16th, and 84th percentiles of the posterior distribution, while the second table block reports the set of parameters that maximise the likelihood. All the priors are log-uniform, and all the parameters are in dimensionless units since the data have been standardised before fitting. The last row reports the Bayesian log evidence of each model clearly disfavouring the Periodic model.

As done in the case of the magnitudes, also the observational times have been standardized³; this operation is done to reduce numerical issues when inverting the covariance matrix Σ .

The DRW model can be generalized by including an additional free parameter $\gamma > 0$ as an exponent to the $|t_i - t_j|/\tau$ term. This is done to provide an alternative that can account for quasar red noise deviating from the DRW model. This model, which we refer to as "Modified DRW", is characterized by the covariance matrix:

$$\Sigma_{ij} = \frac{1}{2} \sigma^2 \tau \exp \left[- \left(\frac{|t_i - t_j|}{\tau} \right)^\gamma \right]. \quad (3)$$

Eqs. (2),(3) refer to pure noise models. When accounting for periodicity, kernels typically include terms proportional to an oscillating function. We define the quasi-periodic oscillation (QPO) kernel as

$$\Sigma_{ij} = \frac{1}{2} \sigma^2 \tau \exp \left(- \frac{|t_i - t_j|}{\tau} \right) \cos \left(\frac{2\pi |t_i - t_j|}{T} \right), \quad (4)$$

containing a multiplicative periodic modulation with period T to the DRW model. The QPO model accounts for a superposition of noise and a periodic signal and, in the limit of $T \rightarrow \infty$, reduces to the DRW model. In the absence of noise, the QPO kernel describes a purely oscillatory process

$$\Sigma_{ij} = \frac{1}{2} \sigma^2 \cos \left(\frac{2\pi |t_i - t_j|}{T} \right), \quad (5)$$

which we refer to as "Periodic" model. The final goal of this work is to measure the robustness of the presence of a periodic signal in the light-curve of J2320+0024. Bayesian statistics is perfectly suited for this task as it allows for precise model selection through the computation of the evidence of a model. The

Bayesian evidence of a model (Z) is the normalization factor of the posterior distribution and, given the same set of data, allows for selecting the preferred among different models. Indeed, given two competing models H_i and H_j , the *Bayes ratio* is:

$$B_{ij} = \frac{p(D|H_i)}{p(D|H_j)} = \frac{Z_i}{Z_j} \quad (6)$$

where we assume that there is no *a priori* preference for H_i over H_j and Z_i/Z_j . The ratio of the model evidences obtained by further marginalising over the entire parameter spaces for H_i and H_j , is called the Bayes factor. If B_{ij} is > 1 (< 1) then model H_i is favoured (disfavoured) compared to H_j . We refer to [Jeffreys \(1948\)](#) for a detailed classification and to [Cocchiararo et al. \(2025\)](#) for a more detailed discussion on GP inference in our astrophysical context.

3.2. Fit and model selection

Since our goal is to estimate the Bayesian evidence of the proposed models, we adopted a nested sampling algorithm for the parameter inference ([Skilling 2004](#)). In particular, following what we did in previous works (e.g., [Rigamonti et al. 2022, 2023](#)), we employed the PYTHON-based implementation RAYNEST ([Veitch et al. 2017](#)), which efficiently computes the marginal-likelihood (Eq. 1) using the GPYTORCH package (see [Gardner et al. 2021](#))⁴. We performed a parameter estimation with 1000 live points, assuming log-uniform priors for all the parameters, except for γ , which is assumed to have a uniform prior. The prior ranges adopted in all the models are reported in Tab. 1.

Fig. 1 shows the best-fit light-curves with the associated errors for the four models discussed in Sec. 3.1: DRW (a), Modified DRW (b), QPO (c), and Periodic (d). In all the plots, the black points represent the data with their associated uncertainties; the solid blue curves and their associated blue shaded area refer to the median, 16th, and 84th model percentiles computed

³ The mean modified Julian date (MJD) is 56766.93, while the standard deviation is 2834.764.

⁴ While Eq. (1) is a marginal-likelihood for a single GP, it is instead to be interpreted as a likelihood when exploring GPs with different parameters.

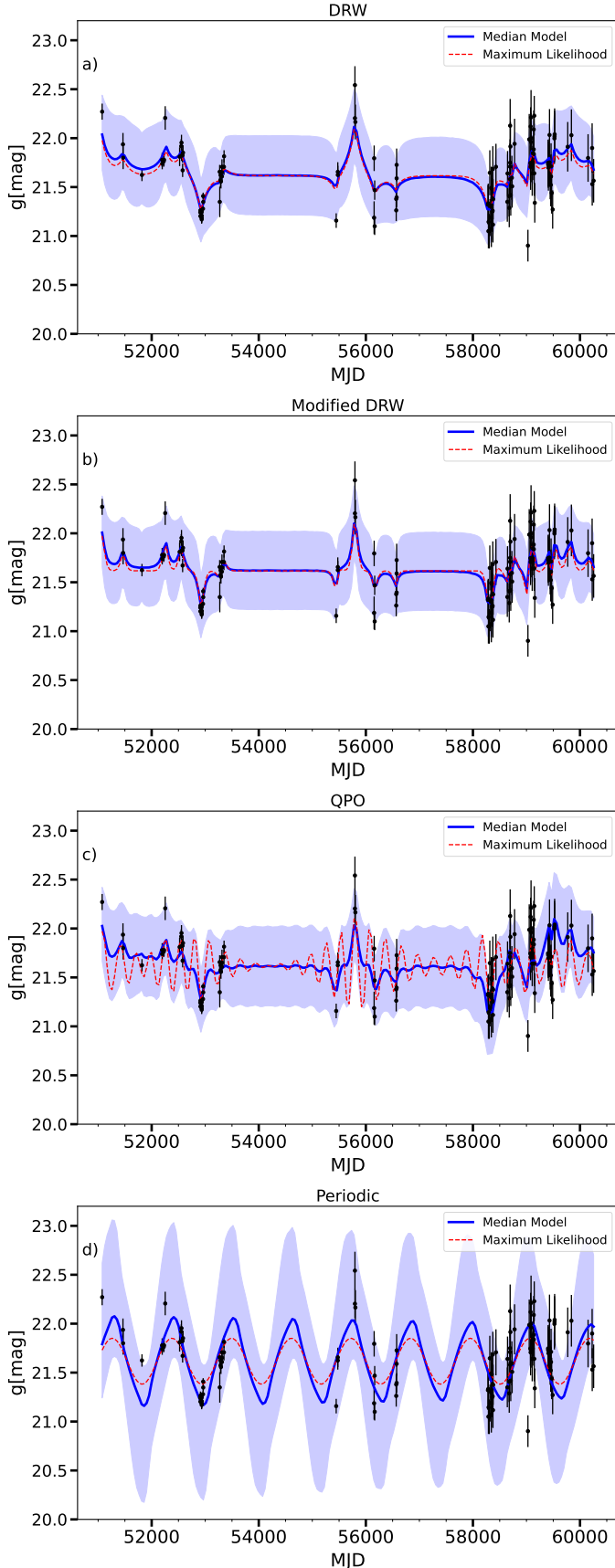


Fig. 1. Best-fit for the g-band light-curve of J2320+0024. The black points represent the data with their errors, the blue solid line and the shaded area represent the median, 16th, and 84th percentiles from the posterior distributions, and the red dashed line refers to the maximum likelihood model. From top to bottom: DRW (a), modified DRW (b), QPO (c), and Periodic (d), we refer to Tab. 1 for the estimated best-fit parameters.

propagating the full shape of the posterior distribution⁵; and, finally, the red dashed curve refers to the model that maximizes the likelihood. The best-fit model parameters (either the percentiles or the likelihood maxima) together with their corresponding Bayesian evidence values are reported in Tab. 1. It is important to clarify that while the maximum likelihood models (i.e., red dashed lines) are obtained using the "Maximum likelihood" parameters reported in Tab. 1, this is not the case for the median, 16th, and 84th models. Indeed, in agreement with our Bayesian approach, the blue lines and the shaded areas presented in Fig. 1 are the median, 16th, and 84th percentiles computed after evaluating the GP model on all the parameter combinations describing the posterior distribution. Fig. 2 displays a comparison of the marginalised posterior distribution of the DRW (blue), Modified DRW (red), QPO (green), and Periodic (orange). The contours of the 2D probability densities are chosen to include 90% of the probability.

Combining the results shown in Fig. 1, Fig. 2, and Tab. 1, allows us to highlight some key insights. Visually, little difference is observed between a DRW (Fig. 1-a) and a Modified DRW (Fig. 1-b). The Bayes factor between the two models is close to 1, indicating no strong evidence in favour of any of the two models. We stress that the DRW model corresponds to the Modified DRW with $\gamma = 1$. In principle, instead of considering γ as a free parameter, we could have fixed it to a value different from 1 (e.g., $\gamma \approx 1.5$). Such a model would have resulted in an only slightly larger evidence (i.e. $\log Z \approx 138.5$), still not indicating a strong preference for either of the two models. Nevertheless, the comparison is useful: the estimated scale length and dispersion are shifted to smaller and larger values, respectively. This indicates that the estimates of τ and σ parameters depend on the high-frequency slope of the assumed power spectrum, possibly suggesting that γ might be included to provide better estimates of the physical parameters (e.g., black hole mass and accretion rate, Arévalo et al. 2023, 2024) regulating the light-curve.

The QPO model exhibits an interesting behaviour. As shown in Fig. 2, its posterior distribution peaks at values of τ and σ that are highly compatible with the ones obtained with the DRW model. However, the period T not only shows a peaked distribution corresponding to $\log_{10} T \approx -1.0$ (i.e., $T \approx 290$ days), but features a very pronounced tail extending toward larger values. This result suggests that, although the peak at $\log_{10} T \approx -1.0$ is well-defined and sharp, the majority portion of the cumulative distribution lies at longer periods. It follows that for values of T comparable or longer than the observational time span, the QPO model becomes insensitive to the oscillatory terms. From a Bayesian statistics perspective, it is not a problem: in cases where a strong periodic signal is present in data, models with ineffective oscillatory terms would contribute negligibly to the posterior and would not influence the final estimate of the best-fit model. However, that is not the case for J2320+0024. Indeed, as shown in Fig. 1-c, the shape of the QPO posterior distribution is also responsible for the difference between the maximum likelihood and the median model.

The red curve demonstrates fast oscillations (i.e., $\log_{10} T \approx -1 \approx 290$ days) while the blue line is much closer to a DRW model. Moreover, the Bayes ratio does not reveal any significant preference between the (modified) DRW and the QPO models, preventing any strong claim in favour of the latter. These findings

⁵ For each set of kernel parameter combination drawn from the posterior distribution, we sample 100 realizations from the GP and we take the median, 16th, and 84th among all the realization on all the set of sampled kernel parameters.

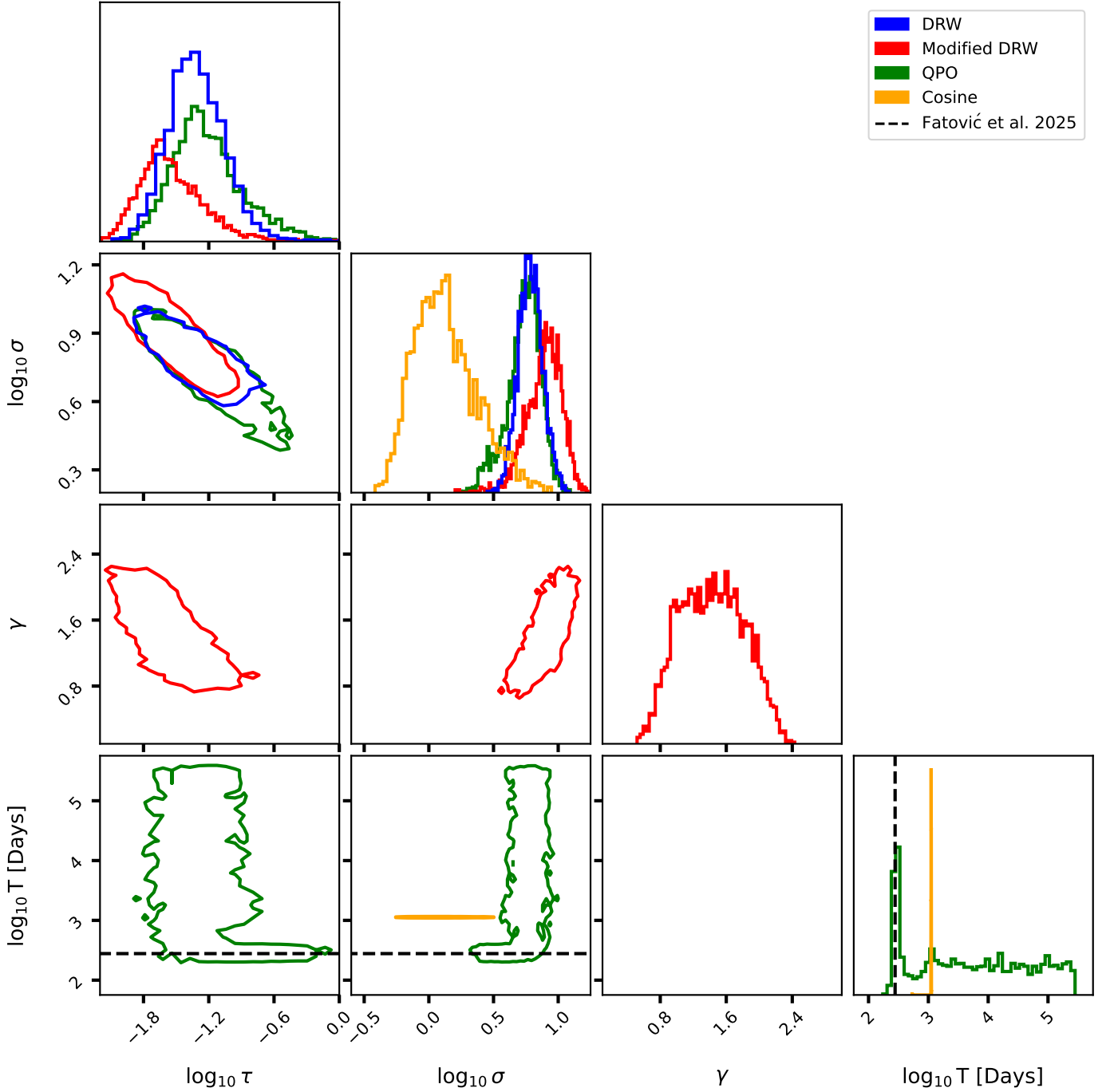


Fig. 2. Corner plot of the posteriors of the different models. DRW is blue, modified DRW is red, QPO is green, and Periodic is orange. Contours are drawn at a level to include 90% of the posterior probability. The black dashed lines refer to the period reported in [Fatović et al. \(2025\)](#). For reasons of clarity, although the fit is performed on standardized data, we report the marginal posterior distribution of the period in units of \log_{10} Days.

suggest a lack of robust evidence for the presence of a periodic signal in the light-curve of J2320+0024.

To compare our results with those found in [Fatović et al. \(2025\)](#) and to assess the potential impact of the overfitting on the QPO model, we also provide a fit with a Periodic model. We note that, unlike the other models considered in this work, the evidence of the Periodic model is significantly smaller. This finding clearly suggests that, analysing the current data, there is no statistical support for preferring the Periodic model over the alternative ones. Thus, there is no strong evidence that the

light-curve of J2320+0024 can be described by a purely periodic signal, underlying the importance of red-noise intrinsic variability. Interestingly, the marginalised posterior distribution reveals extremely sharp peaks in the period ($T \approx 1100$ days) with relative errors smaller than a few percent. Notably, the only peak we find in the period of the Periodic model does not match the main peak identified by the QPO model; instead, it overlaps with a secondary and smaller peak. It is important to notice that the nested sampling algorithms used with the Periodic model detect other peaks, including one that corresponds to the periodicity

reported in [Fatović et al. \(2025\)](#). However, these smaller peaks have significantly lower likelihoods and are therefore rejected by our approach. Since in [Fatović et al. \(2025\)](#) a maximum likelihood approach is adopted and the period search is initialised close to a period of $T \approx 260$ days, it might be possible that the period the authors found in that work corresponds to a local and not a global maximum of the likelihood. Similar conclusions can be drawn by analysing the histogram of the residuals (see Appendix B) among the four models. Although the Kolmogorov-Smirnov test ([Smirnov 1948](#)) indicates that the residuals of the DRW and Modified DRW model always resemble a Gaussian distribution (i.e., p -value > 0.05), this is not true in the case of the Periodic model, and only partially true (i.e., only when using the best-fit model) for the QPO one.

4. Discussion & Conclusion

J2320+0024 has been proposed as a candidate for hosting a MBHB based on modulation of its light-curve ([Fatović et al. 2023](#)). However, the results we obtain following a solid Bayesian approach do not find evidence of a periodic signal in the data. This highlights the importance of preferring statistically robust methods when assessing the nature of variability present in a given source. Nevertheless, the absence of a periodic signal detection in the light-curve of J2320+0024 does not necessarily imply that a MBHB is not present in this source. Our result suggests that, even if such a periodic signal exists, the current data set is too limited in coverage and in robustly detecting it.

Still, we also found a peak in the period for the QPO and Periodic model, which, once translated into physical units, correspond to $T = 290$ days and $T = 1100$ days respectively. [Fatović et al. \(2025\)](#) reported a periodicity of $T \approx 270$ days, much closer to that found by our QPO model. We note that a period of 1100 days is almost an integer multiple of $T = 270$ days (i.e., close to four times larger). Interestingly, when our analysis is extended to the r-band (i.e., the same reported in [Fatović et al. 2025](#)), the detection of the short timescale periodicity (i.e., $T = 290$ days) disappears, while the identification of a longer, statistically unfavoured, peak (i.e., $T \approx 1100$ days) persists. Such changes in the estimation of the period between adjacent broadbands further support the lack of a robust signal in the light-curve of J2320+0024.

We believe that J2320+0024 is a very interesting source that deserves further follow-up observations and analysis, in particular to better characterise the spectral variability reported in [Fatović et al. \(2025\)](#). The authors explained this behaviour within the framework of the PoSKI model ([Popović et al. 2021](#)). This model assumes the presence of a MBHB surrounded by a common BLR, illuminated by the emission of the two mini-discs around each binary component. In this scenario, the appearance of a variable blue or red wing in the MgII is attributed to the binary orbital motion, and it is expected to mirror the periodicity observed in the light-curve. Although this scenario is certainly intriguing, our results challenge it. Indeed, alternative explanations for the observed MgII variability are possible. As discussed in the Sec. 1, several physical mechanisms, such as non-symmetric BLR ([Rigamonti et al. 2025](#)), can produce distorted broad emission profiles, possibly explaining the features observed in the MgII line of J2320+0024. However, explaining the observed variation over time is more challenging. We note that the most significant variation occurs between the SDSS spectrum, obtained about 8 years ago, and the more recent Magellan or Gemini spectra. Over such long timescales, comparable with the BLR dynamical timescales, variations in the shape

of a BEL might be expected, possibly as a result of changes in the morphology or dynamics of the overall BLR. Moreover, the more recent Magellan and Gemini spectra show slight variations among each other; however, those are comparable with the variability of a non-symmetric BLR reverberating after a DRW-like variability of the AGN ([Sottocorno et al. 2025](#)).

We still stress that further photometric and spectroscopic follow-up observations are needed to better clarify the nature of J2320+0024. In particular, as mentioned in Sec. 1, simultaneous modelling of repeated photometric and spectroscopic observations could unveil the true nature of this source. For instance, the light-curve modelling presented here could be extended with a consistent response from perturbed a BLR (e.g., [Rigamonti et al. 2025](#); [Sottocorno et al. 2025](#)) to provide a detailed comparison with modelling or tests based on the MBHB scenario ([Popović et al. 2021](#); [Bertassi et al. 2025](#)).

Acknowledgements

FR acknowledges the support from the Next Generation EU funds within the National Recovery and Resilience Plan (PNRR), Mission 4 - Education and Research, Component 2 - From Research to Business (M4C2), Investment Line 3.1 - Strengthening and creation of Research Infrastructures, Project IR0000012 – “CTA+ - Cherenkov Telescope Array Plus.

MD acknowledge funding from MIUR under the grant PRIN 2017-MB8AEZ, financial support from ICSC – Centro Nazionale di Ricerca in High Performance Computing, Big Data and Quantum Computing, funded by European Union – NextGenerationEU, and support by the Italian Ministry for Research and University (MUR) under Grant ‘Progetto Dipartimenti di Eccellenza 2023-2027’ (BiCoQ). We acknowledge a financial contribution from the Bando Ricerca Fondamentale INAF 2022 Large Grant, *Dual and binary supermassive black holes in the multi-messenger era: from galaxy mergers to gravitational waves*. RB acknowledges support from the ICSC National Research Center funded by NextGenerationEU, and the Italian Space Agency grant Phase A activity for LISA mission, Agreement n.2017-29-H.O. The data underlying this article will be shared on reasonable request to the corresponding author. AS acknowledges the financial support provided under the European Union’s H2020 ERC CoG “B Massive” (Grant Agreement: 818691) and AdG “PINGU” (Grant Agreement: 101142079)

References

- Ackermann, M., Ajello, M., Albert, A., et al. 2015, *ApJ*, 813, L41
- Amaro-Seoane, P., Andrews, J., Arca Sedda, M., et al. 2022, *arXiv e-prints*, arXiv:2203.06016
- Amaro-Seoane, P., Audley, H., Babak, S., et al. 2017, *arXiv e-prints*, arXiv:1702.00786
- Angus, R., Morton, T., Aigrain, S., Foreman-Mackey, D., & Rajpaul, V. 2018, *MNRAS*, 474, 2094
- Arévalo, P., Churazov, E., Lira, P., et al. 2024, *A&A*, 684, A133
- Arévalo, P., Lira, P., Sánchez-Sáez, P., et al. 2023, *MNRAS*, 526, 6078
- Begelman, M. C., Blandford, R. D., & Rees, M. J. 1980, *Nature*, 287, 307
- Bellm, E. C., Kulkarni, S. R., Graham, M. J., et al. 2019, *PASP*, 131, 018002
- Bertassi, L., Sottocorno, E., Rigamonti, F., et al. 2025, *arXiv e-prints*, arXiv:2504.06349
- Britzen, S., Fendt, C., Witzel, G., et al. 2018, *MNRAS*, 478, 3199
- Chambers, K. C., Magnier, E. A., Metcalfe, N., et al. 2016, *arXiv e-prints*, arXiv:1612.05560
- Charisi, M., Bartos, I., Haiman, Z., et al. 2016, *MNRAS*, 463, 2145
- Chen, Y.-C., Liu, X., Liao, W.-T., et al. 2020, *MNRAS*, 499, 2245
- Cocchiararo, F. et al. 2025, in prep
- Covino, S., Landoni, M., Sandrinelli, A., & Treves, A. 2020, *ApJ*, 895, 122
- Covino, S., Sandrinelli, A., & Treves, A. 2019, *MNRAS*, 482, 1270
- Covino, S., Tobar, F., & Treves, A. 2022, *MNRAS*, 513, 2841

- Davelaar, J. & Haiman, Z. 2022, *Phys. Rev. Lett.*, 128, 191101
- De Rosa, A., Vignali, C., Bogdanović, T., et al. 2019, *New A Rev.*, 86, 101525
- D’Orazio, D. J. & Di Stefano, R. 2018, *MNRAS*, 474, 2975
- D’Orazio, D. J., Haiman, Z., & Schiminovich, D. 2015, *Nature*, 525, 351
- Dotti, M., Rigamonti, F., Rinaldi, S., et al. 2023, *A&A*, 680, A69
- Eracleous, M., Boroson, T. A., Halpern, J. P., & Liu, J. 2012, *ApJS*, 201, 23
- Eracleous, M., Halpern, J. P., M. Gilbert, A., Newman, J. A., & Filippenko, A. V. 1997, *ApJ*, 490, 216
- Fatović, M., Ilić, D., Kovačević, A. B., et al. 2025, *A&A*, 695, A208
- Fatović, M., Palaversa, L., Tisanić, K., et al. 2023, *AJ*, 165, 138
- Gardner, J. R., Pleiss, G., Bindel, D., Weinberger, K. Q., & Wilson, A. G. 2021, *GPYtorch: Blackbox Matrix-Matrix Gaussian Process Inference with GPU Acceleration*
- Gaskell, C. M. 1988, in *Active Galactic Nuclei*, ed. H. R. Miller & P. J. Wiita, Vol. 307, 61
- Graham, M. J., Djorgovski, S. G., Stern, D., et al. 2015, *MNRAS*, 453, 1562
- Graham, M. J., Kulkarni, S. R., Bellm, E. C., et al. 2019, *PASP*, 131, 078001
- Hayasaki, K., Mineshige, S., & Ho, L. C. 2008, *ApJ*, 682, 1134
- Ivezić, Ž., Smith, J. A., Miknaitis, G., et al. 2007, *AJ*, 134, 973
- Jeffreys, S. H. 1948, *Theory of Probability*, 2nd edn. (Oxford)
- Jiang, L., Fan, X., Bian, F., et al. 2014, *ApJS*, 213, 12
- Jiang, N., Yang, H., Wang, T., et al. 2022, *arXiv e-prints*, arXiv:2201.11633
- Jovanović, P., Popović, L. Č., Stalevski, M., & Shapovalova, A. I. 2010, *ApJ*, 718, 168
- Ju, W., Greene, J. E., Rafikov, R. R., Bickerton, S. J., & Badenes, C. 2013, *ApJ*, 777, 44
- Kelly, B. C., Bechtold, J., & Siemiginowska, A. 2009, *ApJ*, 698, 895
- Li, Y.-R., Wang, J.-M., Ho, L. C., et al. 2016, *ApJ*, 822, 4
- Li, Y.-R., Wang, J.-M., Zhang, Z.-X., et al. 2019, *ApJS*, 241, 33
- Liu, T., Gezari, S., Ayers, M., et al. 2019, *arXiv e-prints*, arXiv:1906.08315
- Liu, T., Gezari, S., & Miller, M. C. 2018, *ApJ*, 859, L12
- Montuori, C., Dotti, M., Colpi, M., Decarli, R., & Haardt, F. 2011, *MNRAS*, 412, 26
- Montuori, C., Dotti, M., Haardt, F., Colpi, M., & Decarli, R. 2012, *MNRAS*, 425, 1633
- Popović, L. Č., Simić, S., Kovačević, A., & Ilić, D. 2021, *MNRAS*, 505, 5192
- Rasmussen, C. E. & Williams, C. K. I. 2006, *Gaussian Processes for Machine Learning*
- Rigamonti, F., Dotti, M., Covino, S., et al. 2023, *MNRAS*, 525, 1008
- Rigamonti, F., Dotti, M., Covino, S., et al. 2022, *MNRAS*, 513, 6111
- Rigamonti, F., Severgnini, P., Sottocorno, E., et al. 2025, *A&A*, 693, A117
- Roberts, S., Osborne, M., Ebdn, M., et al. 2012, *Philosophical Transactions of the Royal Society of London Series A*, 371, 20110550
- Rosas-Guevara, Y. M., Bower, R. G., McAlpine, S., Bonoli, S., & Tissera, P. B. 2019, *MNRAS*, 483, 2712
- Sandrinelli, A., Covino, S., Dotti, M., & Treves, A. 2016, *AJ*, 151, 54
- Sandrinelli, A., Covino, S., Treves, A., et al. 2018, *A&A*, 615, A118
- Serafinelli, R., Severgnini, P., Braitto, V., et al. 2020, *ApJ*, 902, 10
- Severgnini, P., Ciccone, C., Della Ceca, R., et al. 2018, *MNRAS*, 479, 3804
- Shen, Y., Liu, X., Loeb, A., & Tremaine, S. 2013, *ApJ*, 775, 49
- Skilling, J. 2004, in *American Institute of Physics Conference Series*, Vol. 735, American Institute of Physics Conference Series, ed. R. Fischer, R. Preuss, & U. V. Toussaint, 395–405
- Smirnov, N. 1948, *The Annals of Mathematical Statistics*, 19, 279
- Sottocorno, E., Ogborn, M., Bertassi, L., et al. 2025, *arXiv e-prints*, arXiv:2504.06340
- Storchi-Bergmann, T., Nemmen da Silva, R., Eracleous, M., et al. 2003, *ApJ*, 598, 956
- Tiede, C., Zrake, J., MacFadyen, A., & Haiman, Z. 2024, *arXiv e-prints*, arXiv:2410.03830
- Tsalmantza, P., Decarli, R., Dotti, M., & Hogg, D. W. 2011, *ApJ*, 738, 20
- Valtonen, M. J., Lehto, H. J., Nilsson, K., et al. 2008, *Nature*, 452, 851
- Vaughan, S., Uttley, P., Markowitz, A. G., et al. 2016, *MNRAS*, 461, 3145
- Veitch, J., Del Pozzo, W., Cody, & ed1d1a8d. 2017, *Johnveitch/Cpnest: Pypi Release*
- Verbiest, J. P. W., Lentati, L., Hobbs, G., et al. 2016, *MNRAS*, 458, 1267
- Volonteri, M., Dubois, Y., Pichon, C., & Devriendt, J. 2016, *MNRAS*, 460, 2979
- Wang, L., Greene, J. E., Ju, W., et al. 2017, *ApJ*, 834, 129
- York, D. G., Adelman, J., Anderson, Jr., J. E., et al. 2000, *AJ*, 120, 1579
- Zhu, X.-J. & Thrane, E. 2020, *ApJ*, 900, 117

Appendix A: Analysis on the r-band

In this section, we repeat the same analysis of Sec. 3 on the r-band data of J2320+0024. Also in this case, we tested for different models: DRW, Modified DRW, QPO, and Periodic reporting their best-fit light-curves and parameters in Fig. A.1 and Tab. A.1 respectively⁶.

The overall considerations from the analysis are similar to those discussed for the g-band. The Periodic model is strongly unfavoured, while the DRW, Modified DRW, and QPO have comparable evidence. Notably, in this case, the Bayes ratios between these three models point toward a slight preference for the Modified DRW. Interestingly, while the period found in the Periodic model remains close to that found in the g-band, the main peak in the period of the QPO model is larger and no longer consistent with the one reported by (Fatović et al. 2025) and found by us in the g-band (see Figs. 2, A.2). Such a large variation in the measured periodicities among adjacent bands further probes the lack of a robust periodicity detection in J2320+0024

Appendix B: Quality of the fit

The analysis presented in this paper is based on the Bayes ratio that, as already discussed in the paper, is the most robust approach to model selection and model comparison. However, this statement is true only under the assumption that all the models being compared are a reasonably good description of the data. To check this, we report the standardized residuals (i.e., (model-data)/error) for the same models presented in Fig. 1, testing whether they are consistent with a normal distribution of zero mean and unit dispersion. For each model, we provide the residuals using either the median model (blue) or the model maximizing the likelihood (red), also reporting the mean (μ) and the standard deviation (σ) of the residuals.

In the case of good modelling of the data, the standardized residuals are expected to follow the normal distribution with $\mu = 0$ and $\sigma = 1$. To quantitatively assess this we performed a Kolmogorov-Smirnov test (Smirnov 1948) founding that the DRW and the Modified DRW residuals always follow the expected distribution (p-value larger than the commonly adopted threshold of 0.05), the Periodic model residuals are never normally distributed while the hypothesis of a normal distribution for the QPO model can be accepted only in the case of the maximum likelihood model being compared with the data. Notably, even in this case, the p-value of the QPO model is smaller than that of the DRW or Modified DRW model.

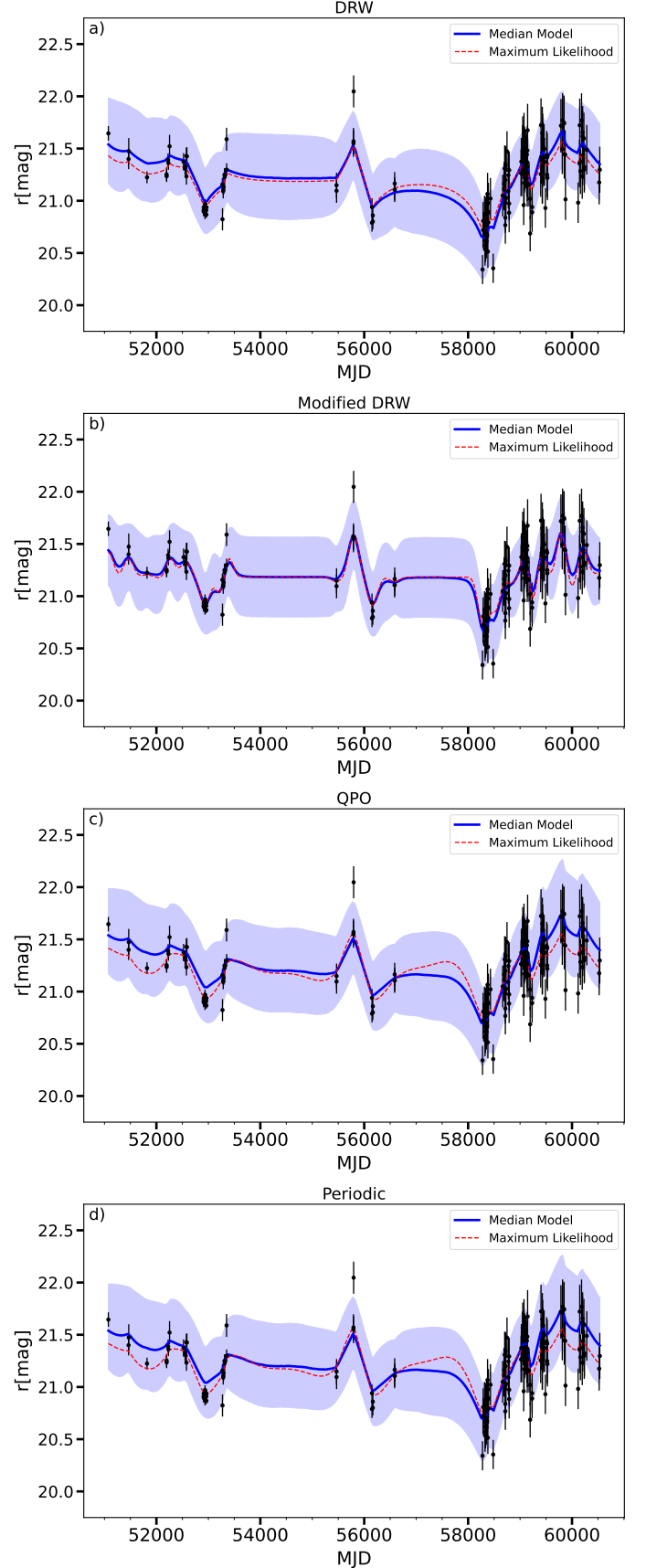


Fig. A.1. Best-fit for the r-band light-curve of J2320+0024. The black points represent the data with their errors, the blue solid line and the shaded area represent the median, 16th, and 84th percentiles from the posterior distributions, and the red dashed line refers to the maximum likelihood model. From top to bottom: DRW (a), modified DRW (b), QPO (c), and Periodic (d), we refer to Tab. 1 for the estimated best-fit parameters.

⁶ Also in this case, we standardized the data using a mean r-band magnitude of 21.182 with a standard deviation of 0.319 and a mean modified Julian date (MJD) of 57602.992 with a standard deviation of 2650.236.

Table A.1. Summary of the different model parameters for the fit to the r-band light-curve of SDSS J2320+0024.

Description	Name	Prior range	DRW	Modified DRW	QPO	Periodic
50th, 16th, 84th Percentiles						
Scale length	$\log_{10} \tau$	$[-3, 1.7]$	$-0.8^{+0.3}_{-0.2}$	$-1.3^{+0.1}_{-0.1}$	$-0.8^{+0.4}_{-0.3}$	-
Dispersion	$\log_{10} \sigma$	$[-3, 1.7]$	$0.5^{+0.1}_{-0.1}$	$0.7^{+0.1}_{-0.1}$	$0.5^{+0.1}_{-0.1}$	$0.01^{+0.3}_{-0.2}$
Slope	γ	$[0.5, 5]$	-	$2.0^{+0.2}_{-0.4}$	-	-
Period	$\log_{10} T$	$[-2, 2]$	-	-	$0.5^{+1}_{-0.7}$	$-0.395^{+0.001}_{-0.001}$
Maximum Likelihood						
Scale length	$\log_{10} \tau$	$[-3, 1.7]$	-0.90	-1.30	-0.73	-
Dispersion	$\log_{10} \sigma$	$[-3, 1.7]$	0.51	0.74	0.44	-0.06
Slope	γ	$[0.5, 5]$	-	2.1	-	-
Period	$\log_{10} T$	$[-2, 2]$	-	-	-0.20	-0.39
log evidence	$\log Z$	-	-163.0	-161.4	-163.4	-275.1

Notes. From left to right, the columns provide a brief description of each parameter, its reference name as used in this work, the assumed prior range, and the best-fit values with their credibility intervals for all the different models. The first table block reports the parameters estimated as the median, 16th, and 84th percentiles of the posterior distribution, while the second table block reports the set of parameters that maximize the likelihood. All the priors are log-uniform, and all the parameters are in dimensionless units since the data have been standardized before fitting. The last row reports the Bayesian log evidence of each model clearly disfavoring the Periodic model.

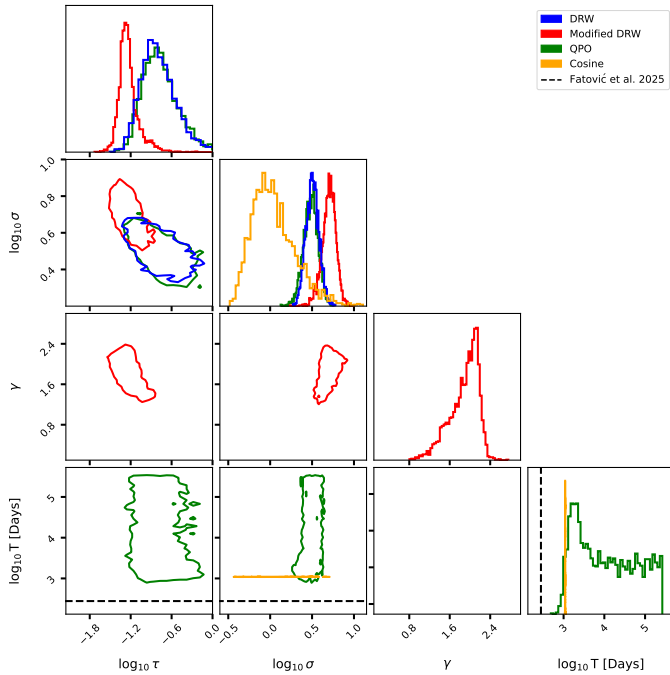


Fig. A.2. Corner plot of the posteriors of the different models. DRW is blue, modified DRW is red, QPO is green, and Periodic is orange. Contours are drawn at a level to include 90% of the posterior probability, while the black dashed lines refer to the period reported in (Fatović et al. 2023). For reasons of clarity, although the fit is performed on standardized data, we report the marginal posterior distribution of the period in units of \log_{10} Days. Please note the different range of $\log_{10} T$ in the corner plot. No short (≈ 260 days) oscillations are identified by the nested sampling algorithm.

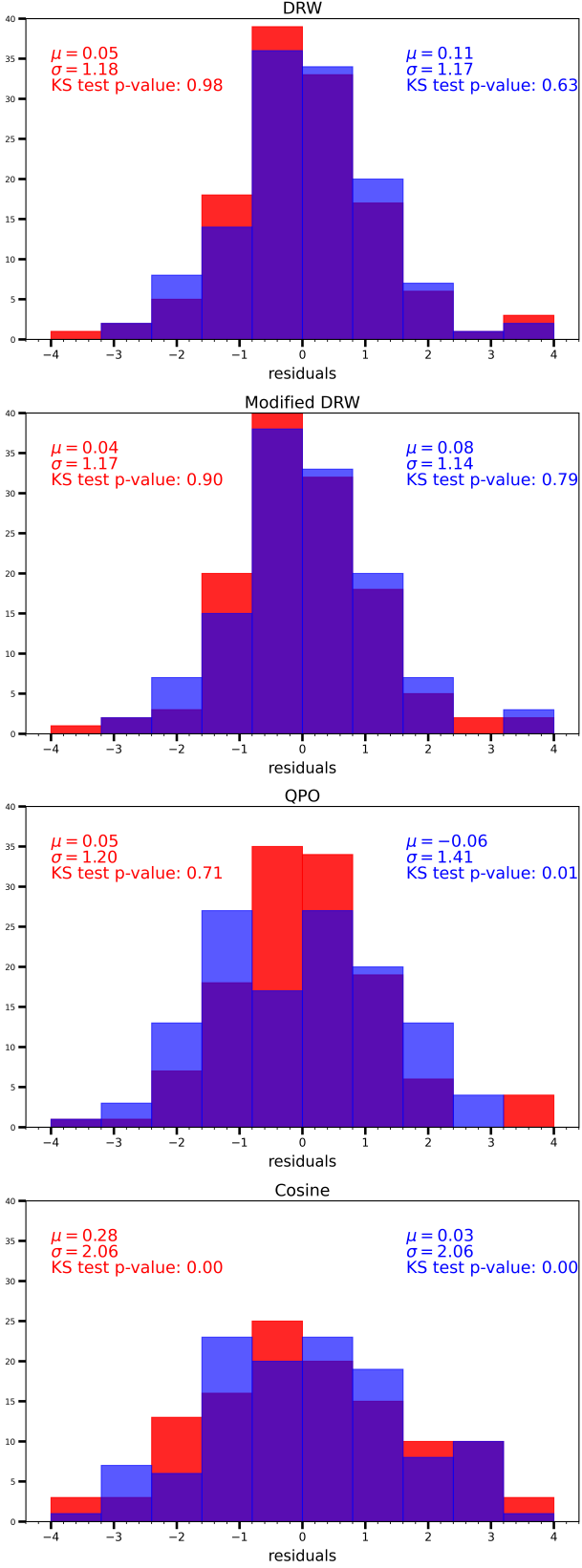


Fig. B.1. Histograms of the residuals (model-data)/error for the models shown in Fig. 1. Each plot also reports the mean, standard deviation, and the p-values of a Kolmogorov–Smirnov test. The color coding follows the one reported in Fig. 1: blue for the residual of the median model, while red for the model which maximizes the likelihood. From top to bottom, we show the DRW, the modified DRW, the QPO, and the Periodic models.